EARTH SURFACE PROCESSES AND LANDFORMS
*Earth Surf. Process. Landforms* **43**, 285–297 (2018)

Published online 14 September 2017 in Wiley Online Library
(wileyonlinelibrary.com) DOI: 10.1002/esp.4244

# Stability of supraglacial debris

**Peter L. Moore***
Department of Natural Resources Ecology & Management, Iowa State University, Ames, IA, USA

Received 29 June 2017; Revised 28 August 2017; Accepted 31 August 2017

*Correspondence to: Peter L. Moore, Department of Natural Resources Ecology & Management, Iowa State University, 339 Science II, Ames, IA 50011, USA. E-mail: pmoore@iastate.edu

ESPL
Earth Surface Processes and Landforms

ABSTRACT: Rock debris on the surface of ablating glaciers is not static, and is often transported across the ice surface as relief evolves during melt. This supraglacial debris transport has a strong influence on the spatial distribution of melt, and is implicated in the formation of hummocky glacial topography in deglaciated terrain. Furthermore, as ice-dammed lakes and ice-cored slopes become increasingly common in deglaciating watersheds, there is rising concern about hazards to humans and infrastructure posed by mass-wasting of ice-cored debris. The existing quantitative framework for describing these debris transport processes is limited, making it difficult to account for transport in mass balance, hazard assessment, and landscape development models. This paper develops a theoretical framework for assessing slope stability and gravitational mass transport in a debris-covered ice setting. Excess water pressure at the interface between ablating ice and lowering debris is computed by combining Darcy's law with a meltwater balance. A limit-equilibrium slope stability analysis is then applied to hypothetical debris layers with end-member moisture conditions derived from a downslope meltwater balance that includes production and seepage. The resulting model system constrains maximum stable slope angles and lengths that vary with debris texture, thickness, and the rate of meltwater production. Model predictions are compared with field observations and with digital elevation model (DEM)-derived terrain metrics from two modern debris-covered glaciers on Mount Rainier, USA. Copyright © 2017 John Wiley & Sons, Ltd.

KEYWORDS: debris; glaciers; meltwater; slope stability; Mount Rainier

## Introduction

Debris cover modifies the relationship between glacier mass balance and climate forcing. Rock debris generally has a lower albedo than debris-free ice, resulting in a net increase in shortwave energy absorption where debris covers a glacier surface. Where debris cover is less than a few centimeters thick, the sun-warmed debris may transfer much of that heat to the ice, increasing ablation rates compared with bare ice (Østrem, 1959; Nicholson and Benn, 2006). However, with increasing debris thickness, more of the absorbed heat is returned to the atmosphere resulting in a net decrease in ablation rate on ice covered with thick debris compared with ablation rate on bare ice.

The effects of debris cover on glacier ablation complicate climate reconstructions and ablation predictions from debris-covered glaciers when ice-margin oscillations deviate from those of other debris-free glaciers (Shulmeister *et al.*, 2009; Vacco *et al.*, 2010; Reznichenko *et al.*, 2011; Rowan *et al.*, 2015; Anderson and Anderson, 2016). Where modern glaciers provide downstream communities with an important freshwater supply, changing debris cover increases uncertainty and complicates water resource planning (e.g. Scherler *et al.*, 2011). Debris-covered glacier termini also frequently host supraglacial and ice-dammed lakes, whose potential for instability and outburst flooding is linked to the ablation of their debris-covered ice dams (Richardson and Reynolds, 2000; Thompson *et al.*, 2012, 2016; Westoby *et al.*, 2016).

Because of the sensitivity of ablation rate to debris-cover thickness, spatially non-uniform debris distribution can generate relief on an ablating ice surface (Benn *et al.*, 2012). Indeed, this relationship is believed to be essential for the genesis of a suite of landforms characteristic of stagnant, debris-laden glacier margins (Benn and Evans, 2010). In particular, hummocky moraine landscapes (Hambrey, 1997) and ice-walled lake-plains (Clayton *et al.*, 2008) are often considered indicative of a glacier with a significant supraglacial debris load that undergoes local supraglacial re-sedimentation during deglaciation (Johnson and Clayton, 2005). However, the process-form linkage that connects ablation of debris-covered glacier margins to hummocky moraine landscapes remains poorly understood.

Two processes of surface ablation have been formally described in debris-covered (and often stagnant) glacier settings: downwasting and backwasting (Krüger *et al.*, 2010). Downwasting is de-icing driven by heat transfer through a stable debris cover, characterized by melt rates that decline with increasing debris thickness. Backwasting occurs where isolated debris-free ice cliffs retreat laterally while shedding undermined debris to the base of the slope (Lawson, 1982). The abundance of backwasting ice cliffs is well known only on a small number of glaciers at a given time, but on a given glacier, they represent a very small fraction of a debris-covered glacier's surface. However, where data is available, local backwasting rates may account for as much as 40% of the net ablation (Schomacker, 2008; Reid and Brock, 2014; Thompson *et al.*, 2016).

Backwasting can only be sustained within a debris-covered glacier where gravitational instability prevents accumulation of debris. In most settings, backwasting occurs on steep ice slopes initiated or maintained by ablation assisted by flowing (supraglacial streams) and standing (supraglacial ponds) meltwater. In some settings, however, debris becomes unstable even on exceptionally gently-sloping ice, apparently due to the accumulation of meltwater within the debris or at the debris–ice interface (Lawson, 1982). While some theoretical descriptions of debris mechanical stability exist for specific cases, a great degree of uncertainty remains about the stability bounds for supraglacial debris.

A more complete understanding of the stability fields of debris-covered ice slopes could help to identify and explain spatial patterns in supraglacial topography and lead to stronger links between supraglacial processes and postglacial landscapes. Similarly, an improved understanding of stability fields may help to discern conditions that favor ablation primarily by downwasting versus ablation enhanced extensively by backwasting. This paper outlines some simple mechanical constraints for debris stability, laying a foundation for further investigations of mass balance and landform genesis in debris-covered glacier settings.

## Background

Glaciers may acquire a blanket of supraglacial debris in several ways. Valley glaciers surrounded by exposed rock may become loaded with rockfall or rock avalanche debris, particularly in settings prone to earthquakes or with weak lithologies. Where valley glaciers form by the confluence of multiple tributaries, medial moraines may form downglacier. These moraines accumulate at the ice surface following melt-out of longitudinal debris bands, which in turn are formed either by the incorporation of sparse rockfall debris at the margins of accumulation basins or by basal and marginal erosion along the inner edge of the tributary valleys (Eyles and Rogerson, 1978; Gomez and Small, 1985; Anderson, 2000). Debris can also be elevated to the surface from lower-level transport in zones of sustained longitudinal compression, such as near the margins of polythermal glaciers or where glaciers encounter adverse bed slopes and obstacles (Hambrey *et al.*, 1999; Moore *et al.*, 2013). In some settings, tephra deposition and windblown debris may contribute significantly, while elsewhere englacial meltwater channels may elevate debris (Spedding, 2000). Though rock avalanche debris may be widespread, it usually remains a discrete superficial source with little relationship to underlying ice structure or dynamics (Shugar and Clague, 2011). In contrast, debris released to the surface at medial moraines and elevated basal ice may connect to a sustained debris source at depth that reflects the internal structure of the glacier (Krüger and Aber, 1999; Kirkbride and Deline, 2013). The spatial arrangement of these debris sources may partly dictate the organization of supraglacial ridges and basins (Evans, 2009). In most settings and regardless of the debris origin, the mean supraglacial debris thickness often increases toward the glacier terminus and with elapsed ablation (Boulton, 1967; Paul and Eyles, 1990).

Glacier researchers have long recognized that thick debris cover buffers ice from surface ablation (Tarr and Martin, 1914, pp. 205–208). However, not until Østrem (1959) performed field experiments on Isfallsglaciären in Swede was the functional impact of debris thickness on ablation rate described. Østrem (1959) found that addition of a thin veneer of debris (less than a few centimeters) caused a slight enhancement of ablation rate compared to clean ice, but that further debris thickening significantly reduced ablation rate. Subsequent studies of *in situ* (Conway and Rasmussen, 2000; Krüger and Kjær, 2000; Takeuchi *et al.*, 2000; Schomacker and Kjær, 2007; Mihalcea *et al.*, 2008) and laboratory (Reznichenko *et al.*, 2010) debris-covered ice ablation have corroborated these findings, and the effect has been reproduced in a recent mechanistic model (Evatt *et al.*, 2015).

The sensitivity of ablation to debris thickness has important implications for the creation of topographic relief on the ice surface. If debris were stationary atop ice undergoing subdebris ablation, all of the debris would be laid down passively as melt-out till and would preserve some evidence of the debris concentration, texture, and structure within the parent glacier. However, where topographic relief exists in supraglacial settings, debris is often transported away from its original melt-out or accumulation site, eliminating much of the debris' sedimentological properties inherited from its original subaerial emplacement and modifying its spatial distribution (Lawson, 1982). Relief can be created on a debris-covered glacier surface by at least three mechanisms: (1) crevasse formation or other structural features developed through active ice flow or fracture (Bennett *et al.*, 2000); (2) localized melting through contact with meltwater flowing in supraglacial channels or standing in supraglacial lakes (Pickard, 1983); (3) differential melting caused by spatial variations in debris thickness or thermal conductivity (Nicholson and Benn, 2013). The dominance of any one of these processes in generating relief and promoting debris transport may vary from one glacier to another, or with position on a single glacier.

A variety of mass transport processes and forms have been described in a range of supraglacial settings, manifested as both steady and episodic transport across the ice surface. These mass movement processes in debris-covered ice have been described by several authors, including Sharp (1949), Lawson (1979), Eyles (1979), Paul and Eyles (1990), and Krüger *et al.* (2010), and include topples, slides, and flows that in most ways operate in a manner analogous to their non-glacial counterparts (Selby, 1993). However, the presence of a 'slippery', impermeable ice substrate that provides a persistent source of meltwater to the base of the debris represents an important departure from conditions in other familiar settings, and merits separate analysis.

### Ablation phenomena

Among the most lucid early field descriptions of the coupling between ablation and mobile supraglacial debris was given by Robert Sharp in his study of Wolf Creek Glacier (now known as Steele Glacier), Canada (Sharp, 1949). Sharp (1949) noted the effect of non-uniform debris thickness on the ablation rate and its link to the creation of supraglacial relief. He was among the first to explicitly connect the transport of supraglacial debris into supraglacial basins to the topographic inversion posited to happen during final de-icing and formation of hummocky moraine. Sharp (1949) also recognized that the relief generated by differential ablation itself caused re-distribution of supraglacial debris. The resulting thinning of the debris on supraglacial hills and thickening in the basins eventually reversed the ablation differential and dampened the relief. Sharp (1949) posited that this reversal process limited supraglacial relief to 150 feet on Wolf Creek Glacier. He further noted that these supraglacial transport processes resulted in progressive fining and sorting of supraglacial debris with transport, highlighting the roles of meltwater transport and sorting of fines as well as crude slope-scale sorting of coarser debris due to talus-like transport.

Subsequent observations and measurements have corroborated Sharp's (1949) observations, while revealing additional

insights into the relationships between supraglacial debris distribution and re-distribution and ablation of underlying ice (Eyles, 1979; Kjær and Krüger, 2001; Schomacker, 2008; Krüger *et al.*, 2010; Bennett and Evans, 2012). Eyles (1979) distinguished three facies of supraglacial debris deposits, combining direct observations with inferences from sediment properties to connect debris characteristics with transport processes. A group of studies on the Klutlan Glacier in south-western Yukon, Canada, also recognized the important links between ablation and local debris re-distribution while seeking a modern analogue to the ice-marginal processes responsible for the late Wisconsinan landscape of the southern Laurentide ice sheet margin (Driscoll, 1980; Watson, 1980; Wright, 1980). Work on various glaciers in Iceland has more recently sought to quantify – over the course of the wastage process – the contributions of downwasting, slope retreat, backwasting, and basal melt on the long-term rate of de-icing and effects of different debris transport processes (Kjær and Krüger, 2001; Schomacker, 2008; Schomacker and Kjær, 2008; Krüger *et al.*, 2010; Korsgaard *et al.*, 2015). In general, these studies indicate that although debris-free slopes represent a relatively small areal fraction of most debris-covered glacier surfaces, they account for a significant portion of total ablation. Subsequent work has largely concentrated on the energetics of downwasting and backwasting with little attention focused on the mechanics of debris re-distribution.

### Debris re-distribution

The most detailed studies of supraglacial re-sedimentation phenomena and their resulting sedimentary signatures are those of Lawson (1979, 1982) on the terminus of Matanuska Glacier, Alaska. These studies highlighted the processes by which liquefied sediment gravity flows re-distributed debris over the ablating ice surface, and the impact of the re-sedimentation processes on measured till properties such as deposit morphology and particle fabric. In addition to describing the impact of the glacier's debris cover on ablation, Lawson (1982) described four different types of sediment-gravity flows that differed in texture and moisture content, and whose dynamics differed substantially.

Lawson (1982) recognized the significance of excess water pressure in enabling flow mobilization even on slope angles of just a few degrees. The excess water pressure was explained by analogy with thawing permafrost, using a thaw-consolidation model (Morgenstern and Nixon, 1971; McRoberts and Morgenstern, 1974a). Lawson's (1982) thaw-consolidation approach to studying supraglacial debris mobilization was expanded upon and generalized by Paul and Eyles (1990). The premise of the thaw-consolidation model in supraglacial settings is that the release of debris upon ablation causes compaction, driving meltwater out of constricting pore space. By analogy with geotechnical consolidation theory, excess pore pressures are computed as a function of the thaw-consolidation ratio $R$, which describes the ratio between a melt-rate parameter $\alpha$ and a coefficient of consolidation $c_v$, which depends on the decrease in porosity that occurs during consolidation ($R = \alpha/\left(2\sqrt{c_v}\right)$) (Morgenstern and Nixon, 1971). The excess pore pressure generated by this process $u_e$, normalized to the submerged weight of debris per unit area, can be expressed as:

$$\frac{u_e}{\gamma' h} = \frac{1}{1 + \left(\frac{1}{2R^2}\right)}, \tag{1}$$

where $\gamma' = \gamma_m - \gamma_w$ is the submerged unit weight of the debris of thickness $h$, $\gamma_m$ is the moist unit weight of debris, and $\gamma_w$ is the unit weight of water. Note that the total pore pressure $u$ is the sum of excess pore pressure and the hydrostatic pressure under depth $d$ of water, $u = \gamma_w d + u_e$. When $R$ is large (corresponding roughly to a rapid rate of thaw relative to the rate of dissipation of excess pore pressure) the quantity on the right-hand side of Equation (1) approaches unity and excess pore pressure approaches the effective stress under hydrostatic conditions. Conversely, when $R$ is small (slow melt rate or fast pore-pressure dissipation) the right-hand side approaches zero and excess pore pressure is negligible.

The thaw-consolidation model was developed for permafrost settings, and was adapted with little modification to ablation in debris-laden glaciers. In its original form, the model boundary conditions require that all pore-fluid flow away from the melting front is accompanied by soil volume change, while volume change is specified through a compressibility parameter derived from geotechnical tests on consolidating unfrozen debris (Muir Wood, 2009). While these assumptions and conditions may be adequate for describing debris instability due to permafrost thaw (McRoberts and Morgenstern, 1974b), and perhaps for instability atop ablating debris-rich glacier ice (Paul and Eyles, 1990), they are more problematic for sub-debris ablation in most glacial settings, where debris concentrations are usually less than a few percent by volume. The parameters that characterize the volume contraction of a soil and corresponding pore-pressure development and dissipation are strictly meaningful only in connection with the laboratory experiments from which they are derived and attain questionable meaning when the pore-filling material (ice in this case) precludes any load-supporting grain network prior to ablation. Furthermore, in relatively debris-poor (i.e. most) glacier ice, accumulation of newly-thawed debris to the base of an overlying debris layer takes place at a rate that is small compared to the evacuation of meltwater required. For these reasons, a separate analysis of water–debris interaction is required to describe supraglacial debris stability accurately in a wider range of glaciological settings.

This paper presents a general mechanical framework for the interaction of meltwater and supraglacial debris in supraglacial settings with the objective of enabling modeling of ice surface evolution and debris transport over timescales of weeks and longer. While there are likely some important debris transport processes that operate on debris-covered slopes that are not at the limits of gravitational stability (e.g. creep, slopewash, glaciofluvial and aeolian processes) (e.g. Anderson, 2000), gravitational instability is assumed to accommodate a significant fraction of – if not most – initial mobilization and transport. Therefore, the analysis shown here in this paper focuses on the identification and application of the threshold for instability on moist, debris-covered ice slopes undergoing ablation.

## Model Development

The mechanical framework developed here follows from water mass balance and from limit-equilibrium theory for slope stability on thawed unconsolidated soils. For simplicity, gravitational stability is assessed in terms of steady-state stresses and water pressures, while transients are qualitatively discussed in terms of perturbations to steady-state conditions. This is justified in part by appealing to the fact that meltwater may be supplied steadily to the base of a debris-layer if the debris is sufficiently thick (Reznichenko *et al.*, 2010). Rain and snowmelt events may certainly trigger instability as well, but in the framework proposed herein, their transient impact may be viewed as a supplemental meltwater source. Indeed,

where slope angle is small, the transient impact of rainfall loading is usually to increase resisting forces more strongly than driving forces are increased (Lu and Godt, 2013, pp. 336–338).

In contrast with Lawson (1982) and Paul and Eyles (1990), it is assumed here that the rate of volume growth in debris thickness via ablation is small compared to the rate of meltwater generation. This assumption enables neglect of changes in debris thickness, which is appropriate for ablation of ice with small or zero debris concentration.

## Downwasting equilibrium

The removal of ice from beneath a debris mantle without destabilizing the debris requires both the expulsion of water from the debris–ice interface and gravitational settling of the debris itself. To sustain local equilibrium, it is assumed that a slope-normal hydraulic gradient is established through the debris that is sufficient to drive pore-water flow away from the ablating interface as rapidly as it is produced. If, however, the pore-water pressure at the debris–ice interface equals or exceeds the weight per unit area of the overlying debris, instability may ensue. The first requirement for stability is therefore that the water pressure developed at the debris–ice interface to drive water through settling debris is less than the debris overburden.

First consider the simplest case of a near-horizontal debris-covered ice surface experiencing steady melt and a fixed water table at a height $d$ above the debris–ice interface (Figure 1a). Meltwater may be driven away from the ablating interface and through settling debris according to Darcy's law in one dimension, $q_z = K_s \mathrm{d}H/\mathrm{d}z$, where $K_s$ is saturated hydraulic conductivity, $H$ is the total hydraulic head and $z$ is the vertical coordinate. Assuming that the pore-water pressure $u$ at the water table surface is zero at height $d$ above the debris–ice interface (defined as datum), the total hydraulic head at the debris surface $H = d$. At the debris–ice interface, the elevation head is zero and the pressure head is $u/\gamma_w$. Darcy's law for upward seepage driven by a linear hydraulic gradient may accordingly be written:

$$q_z = K_s\left(\frac{u}{\gamma_w d} - 1\right). \tag{2}$$

When $u = \gamma_m h$, fluid pressure supports the full weight of the debris, and the debris loses all frictional coupling to the underlying ice. The ratio $r_u$ is sometimes referred to as the pore-pressure ratio ($r_u = u/\gamma_m h$), and it may be surmised that the debris is only stable for $r_u \leq 1$.

Mass conservation of water in the $z$ direction requires that $q_z = \dot{m}$, so Equation (2) may be combined with the definition for $r_u$ into a non-dimensional stability bound:

$$r_u = \frac{\gamma_w d}{\gamma_m h}\left(1 + \frac{\dot{m}}{K_s}\right). \tag{3}$$

As expected, for zero melt rate the pore-pressure is hydrostatic. However, any finite meltwater production requires development of an excess water pressure at the debris–ice interface that increases with decreasing debris permeability. The magnitude of this excess pressure is simply $\gamma_w d\,\dot{m}/K_s$. At this point in the analysis, we acknowledge that there should be some dependence of $d$ on $\dot{m}$, but this relationship must remain unspecified until a slope-parallel water balance can be defined. This problem is considered in a separate section later.

For the simplest case where the water table height is fixed at the debris surface ($d = h$), and for typical wet debris properties, the term outside the parentheses on the right-hand side of Equation (3) is in the range 0.4–0.6. The ratio of melt rate to saturated hydraulic conductivity must therefore be less than this value to prevent instability for any configuration of debris over ice.

This simple linear relationship between $\dot{m}/K_s$ and excess pore pressure is illustrated for arbitrary debris properties in Figure 2 along with a solution to the much more complex thaw-consolidation model used by Lawson (1982). The excess pore pressure in both models is normalized in Figure 2 to the submerged unit weight for consistency. However, the quantity on the horizontal axis differs between the two lines, and since there is no intrinsic relationship between $R$ and $\dot{m}/K_s$, no direct comparison can be made. Nevertheless, both models indicate qualitatively similar behavior over much of the domain of the independent variable. However, the thaw-consolidation model generates normalized excess pressures that only approach one asymptotically, suggesting that thawing debris cannot completely lose its strength. In contrast, the ablation-settling model rapidly approaches and becomes equal to one, suggesting that for some finite value of the ratio $\dot{m}/K_s$, vertical seepage forces can fully oppose the weight of the debris and the debris can become fully fluidized.

While fluidization may occur for $r_u = 1$ (and $r_u > 1$ is arguably non-physical), smaller values of $r_u$ may still promote instability if the water pressure at the debris–ice interface reduces frictional strength sufficiently. A first-order estimate of this stability constraint may be assessed through an infinite slope analysis.

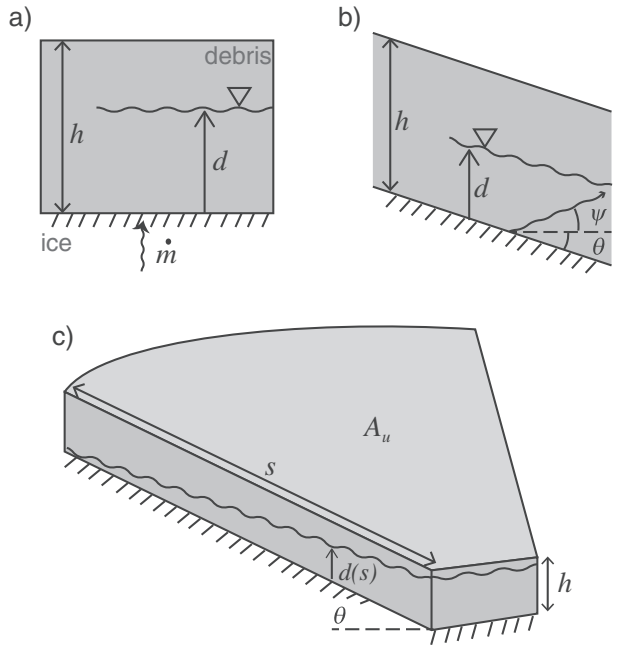


**Figure 1.** Schematic illustrations of model systems including supraglacial debris (gray shading) settling atop ablating ice (hachured). Water table indicated by wavy line. (a) Ablation-settling system with debris thickness $h$ and pore-water depth $d$ and ablation rate $\dot{m}$; (b) infinite slope with slope angle $\theta$ and seepage vector inclined an angle $\psi$ (increasing upward) from horizontal; (c) finite slope with pore-water depth a function of distance downslope $s$ and upslope accumulation area $A_u$.

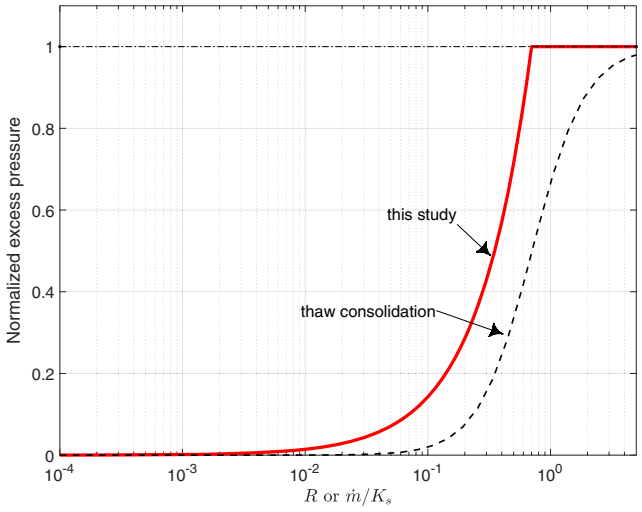


**Figure 2.** Comparison between ablation-settling and thaw-consolidation models of normalized excess pore pressure. The horizontal axis is $R$ for the thaw-consolidation model (dashed black line) and $\dot{m}/K_s$ for the ablation-settling model presented here (red). Note that these horizontal axis values are not directly related, and both model are plotted for the purpose of qualitative comparison. [Colour figure can be viewed at wileyonlinelibrary.com]

## Infinite slope analysis

When there is a non-zero frictional resistance to slip at the base of the debris layer, comparison of driving and resisting stresses can suggest the conditions under which the slope may become unstable. A widely-used approach to this type of problem is the infinite slope analysis. The infinite slope analysis requires a key assumption that the depth to failure in the slope under consideration is small compared to the slope length, so that longitudinal forces (e.g. buttressing from the footslope below) are negligible compared to the driving and resisting forces that arise locally from the debris self-weight. Additionally, the static intergranular friction angle in most supraglacial debris likely exceeds the effective friction angle at the debris–ice interface (e.g. Barrette and Timco, 2008), ensuring that initial failure will occur at the interface rather than within the debris. Most modern debris-covered ice settings satisfy the assumptions of the infinite slope analysis better than many non-glacial hillslopes, making the infinite slope analysis particularly suitable for the present purpose.

The infinite slope analysis is often formalized through the use of a 'safety factor' $F$, defined as the ratio of the stresses that resist failure and those that promote failure at the expected slip interface. When $F>1$, the slope is expected to be stable, whereas if $F\leq 1$, the slope should be unstable. The derivation of the slope-stability criterion is provided by many sources (e.g. Lambe and Whitman, 1969; Muir Wood, 2009), so it is simply stated here:

$$F = \frac{\mu(\cos^2\theta - r_u)}{\cos\theta \sin\theta}, \tag{4}$$

where $\theta$ is the slope angle (Figure 1b) and the friction coefficient for sliding along the debris–ice interface $\mu$ is assumed to be known (~0.5; Barrette and Timco, 2008). When the debris is dry ($r_u=0$) or seepage is vertically downward (Muir Wood, 2009), Equation (4) reduces to the familiar $F=\mu/\tan\theta$, which is to say that the upper bound for a stable slope angle is simply the effective friction angle of the sliding interface $\tan^{-1}(\mu)$. However, where $r_u$ is greater than zero, the steepest stable slope angle is reduced according to Equation (4).

The infinite slope idealization can be modified to account for any seepage direction, provided that it is constant along the slope. Defining $\psi$ as the inclination (increasing upward from horizontal in the downslope direction; Figure 1b) of the seepage vector, $r_u$ for arbitrary seepage orientation is (Muir Wood, 2009):

$$r_u = \frac{\gamma_w d}{\gamma_m h}\frac{\cos\theta\cos\psi}{\cos(\psi+\theta)}. \tag{5}$$

Since the current model framework permits meltwater input only from the debris–ice interface, any finite melt supply $\dot{m}$ requires divergence of the seepage direction from the slope angle ($\psi \neq -\theta$). Assuming that both the slope-normal and slope-parallel components of seepage can be expressed in linear terms via Darcy's law, the seepage vector is simply the vector sum of its slope parallel and slope normal components, and its deviation from slope-parallel $\beta=\theta+\psi$. The seepage angle $\psi$ is therefore:

$$\psi = \tan^{-1}\left(\frac{\dot{m}}{K_s \sin\theta}\right) - \theta, \tag{6}$$

where $K_s\sin\theta = v_s$ is the downslope (one-dimensional) Darcy flow velocity [$L\,T^{-1}$]. With this definition, it can be shown that $r_u$ as expressed in Equation (3) is a special case of Equation (5).

Taking $F=1$ to define the stability bound in Equation (4) and solving for $r_u$ yields a non-dimensional expression for the critical pore-pressure ratio, this time for slope angles $\theta>0$:

$$r_u = \cos^2\theta - \frac{\cos\theta\sin\theta}{\mu}. \tag{7}$$

This expression may then be set equal to the right-hand side of Equation (5) to find critical values of seepage direction (and by extension the ratio $\dot{m}/K_s$) at the threshold of instability. As in the case with $\theta=0$, the water pressure at the interface approaches hydrostatic when $\theta$ and the ratio $\dot{m}/K_s$ are small. Under those circumstances, the maximum stable value of $r_u$ is related to the ratio of water to debris unit weights, which will generally fall in the range 0.4–0.6. For larger values of $\dot{m}/K_s$, significant excess water pressures ($u>\gamma_w d$) may develop, and even on very gentle slopes, debris may become unstable.

The assumption – thus far taken for granted – of a spatially-uniform steady-state water-table height $d$ in the presence of steady melt and slope-normal seepage is unrealistic without meltwater removal from the debris surface or downslope seepage. The next section accounts for the downslope dimension of the water balance, providing an approximate framework for stability analysis that can be applied in more realistic glacier settings.

## Finite slope stability

On a hillslope receiving a sustained, distributed supply of water, the steady-state water table height varies according to position on the hillslope. Numerous authors have developed simple models that balance groundwater recharge and flux through idealized surface aquifers in real or synthetic terrain (O'Loughlin, 1986; Montgomery and Dietrich, 1994; Talebi *et al.*, 2008). Such models can be used, with some caveats, to predict the downslope component of a hillslope water balance

and thereby estimate the slope lengths, slope angles, or slope positions at which instability may occur.

Our analysis begins with a steady-state balance of water in an idealized hillslope according to a reference frame fixed to the ablating debris–ice interface, and assume that water pressure is approximately hydrostatic throughout (Figure 1c). The volume of meltwater produced in unit time on the slope is $\dot{m}A_s$, where $A_s$ is the ablating surface area. Once produced by ablation, meltwater moves downslope according to a per-unit-width form of Darcy's law:

$$q_s = v_s d = K_s d \frac{\mathrm{d}H}{\mathrm{d}s}, \tag{8}$$

where $q_s$ is downslope discharge per unit width [$L^2\,T^{-1}$], the product $K_s d$ is the effective aquifer transmissivity, and $s$ is the downslope coordinate ($s = x/\cos\theta$). If the hydraulic gradient is constant along slope and seepage is approximately slope-parallel, the gradient term in Equation (8) can be replaced by $\sin\theta$ (Montgomery and Dietrich, 1994). Mass conservation for steady state melt requires that the downslope discharge equals the melt from all the upslope ablation, $\dot{m}A_u$, where $A_u$ is the upslope hydrological contributing area (O'Loughlin, 1986). When $A_u$ is normalized to unit width, it is equivalent to the specific upslope contributing area, $a$, with dimensions of [$L$]. For a straight slope, $a = s$, the downslope water balance becomes $\dot{m}s = K_s d \sin\theta$, which may be solved for $d$ to yield the steady-state height of the water table as a function of position on the slope:

$$d = \frac{\dot{m}s}{K_s \sin\theta}. \tag{9}$$

To allow for more complex slope shapes or application in real terrain analysis, $s$ may be replaced by $a$ without loss of generality. In this case, the ratio $\dot{m}a/K_s d \sin\theta$ is analogous to the 'wetness' parameter of Montgomery and Dietrich (1994).

Under the assumption of slope-parallel seepage ($\theta = -\psi$ in Equation (5)), $r_u = (d\gamma_w/h\gamma_m)\cos^2\theta$ and the expression for factor of safety may be re-written:

$$F = \left(1 - \frac{d}{h}\frac{\gamma_w}{\gamma_m}\right)\frac{\mu}{\tan\theta}. \tag{10}$$

This expression is nearly identical to those of Montgomery and Dietrich (1994) and Talebi *et al.* (2008), who used it to predict zones of instability in real and synthetic landscapes, respectively. Substituting Equation (9) into Equation (10) for $d$ yields:

$$F = \left(1 - \frac{\dot{m}s\gamma_w}{hK_s \sin\theta\gamma_m}\right)\frac{\mu}{\tan\theta}. \tag{11}$$

This relationship is illustrated in Figure 3, where $F$ is plotted as a function of $\theta$ for various values of $\dot{m}/K_s$, with $s/h = 300$, $\mu = 0.5$, and $\gamma_w/\gamma_m = 0.59$. Note that the range of stable slope angles gets smaller with increasing $\dot{m}/K_s$, and that under most conditions there exists a range of non-zero slope angles that are more stable than both steeper and more gentle slopes. Note also, however, that Equations (10) and (11) are only valid for $d \leq h$. Where $d > h$, the debris is fully saturated and any additional meltwater accumulation results in runoff. Under these circumstances, if gravitational instability has not yet mobilized debris, entrainment by concentrated overland flow may do so. The analysis of overland flow erosion is beyond the scope of the current treatment, and settings where the debris is fully saturated are simply identified here as susceptible to hydraulic erosion.

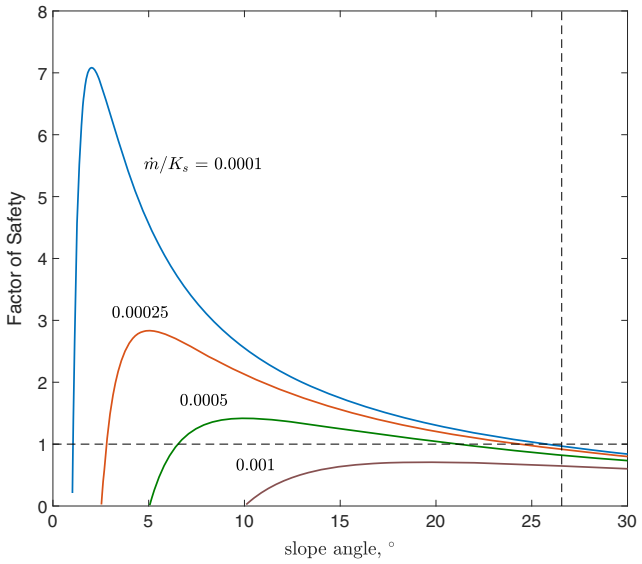


**Figure 3.** Factor of safety as a function of slope angle for the infinite slope model, with four different reasonable values of $\dot{m}/K_s$ and $\mu$ assumed to be 0.5. [Colour figure can be viewed at wileyonlinelibrary.com]

Although similar models have been used in terrestrial hillslope settings (Montgomery and Dietrich, 1994; Borga *et al.*, 1998; Casadei *et al.*, 2003; Talebi *et al.*, 2008), this model is not strictly a permissible extension of the linear hillslope water balance or the infinite slope stability analysis. When the seepage vector is significantly inclined relative to slope-parallel, pore pressures in excess of hydrostatic may develop. The expression for $F$ could presumably be modified by using Equation (5) for $r_u$ with $d$ from Equation (9). However, this modification would violate the assumption that permits use of the linear Darcian flow model in finite slopes (flow parallel to the slope and driven by elevation head gradient). This approach is therefore risky, and the finite slope analysis should be limited to cases that may be approximated by slope-parallel water flow and hydrostatic pressures. These cases will be those for which excess water pressure is negligible and $r_u$ is approximately hydrostatic.

Among the key assumptions of the infinite slope stability model is the provision that the longitudinal forces acting on the debris control volume from upslope and downslope are balanced. If pore pressure is permitted to vary with position along slope and the resisting stress varies correspondingly, it is conceivable that a force imbalance could arise in the model. This circumstance may be limited to settings where the lower portions of slopes become unstable, or where slope angle varies along slope. In the former case, the extension of the infinite slope idealization to finite slopes should be understood to supply an upper bound on slope length, as well as slope angle. For the latter case, a more rigorous approach involving either analytical hillslope forms (e.g. Talebi *et al.*, 2008) or numerical solutions may be an alternative. Despite these limitations, I suggest that the model outlined earlier may be used broadly to identify first-order spatial constraints, debris characteristics, and climate regimes that influence the stability and transport of supraglacial debris, and consequent effects on ablation rates and debris sedimentation.

## Model Application

A framework has been introduced to estimate the bounds of stability for supraglacial debris in idealized settings. To be

useful, the model framework must make predictions that help to explain observations in the field, and must be readily applied to real debris-covered ice masses. To demonstrate the application of this model, simple terrain metrics were retrieved through analysis of high-resolution (3 m LiDAR [Light Detection and Ranging]-derived [Puget Sound LiDAR Consortium, 2009]) digital elevation data from two partly-debris-covered glaciers in the western United States: Carbon Glacier and Emmons Glacier, Washington State (Figure 4).

Emmons Glacier is among the largest glaciers in the lower 48 US states (area ~ 11 $km^2$ [Sisson *et al.*, 2011]), and flows northeast from the summit of Mount Rainier. Carbon Glacier (area ~ 9 $km^2$ [Sisson *et al.*, 2011]) flows north from Mount Rainier, and while similar in total ice volume, extends to lower elevations. Except for a break in slope at the very terminus, Carbon Glacier has a much gentler downglacier surface slope than Emmons. Both glaciers have extensive debris cover over much of their termini (Emmons debris cover ~20% of glacier area; Carbon debris cover ~34%), though Carbon Glacier's debris cover is derived predominantly from rockfall from the adjacent volcanic edifice (Willis Wall), while a significant portion of Emmons Glacier's debris blanket derives from the emergence and concentration of medial moraine debris. The difference in debris sources leads to greater englacial control and apparent organization of supraglacial topography on Emmons Glacier compared with Carbon Glacier. A team led by the author made observations and measurements of supraglacial debris on Emmons Glacier during July and August of 2013 and 2014.

Using the open-source terrain analysis software Whitebox GAT (Lindsay, 2016), a 3 m bare-earth digital elevation model (DEM) was constructed from the last-return point cloud from a 2007–2008 LiDAR campaign conducted by the Puget Sound LiDAR Consortium (2009). The statistics and spatial distribution of surface slope $\theta$ and specific catchment area $a$ were computed for both debris-covered termini (Figure 4), and are plotted in slope–area diagrams analogous to those in Montgomery and Dietrich (1994) in Figure 5. One result that stands out is the paucity of horizontal surfaces and the abundance of surfaces sloping between 10° and 15° (Figure 4b), a pattern that holds for both glaciers despite their different debris sources, downglacier slopes, and internal structures.

In the analysis presented earlier, debris instability may arise by three mechanisms. The first mechanism is complete strength

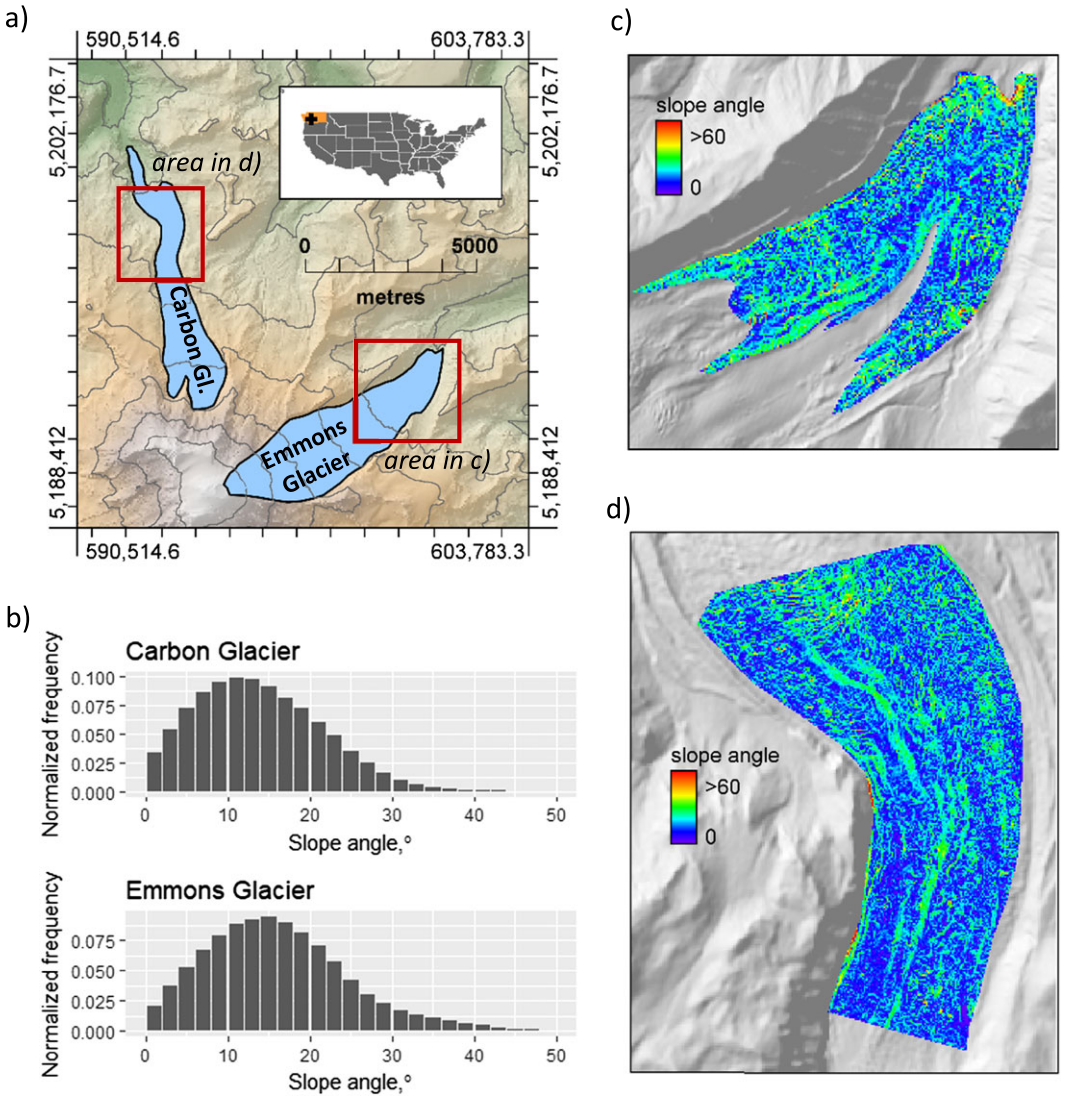


**Figure 4.** Surface slopes of two debris-covered glaciers on the north and east slopes of Mount Rainier, Washington, USA. (a) location map of Carbon Glacier and Emmons Glacier with boxes showing the extent of panels c and d; inset shows the location of Mount Rainier in the southwest part of Washington state; (b) histograms of slope angle normalized frequency for the areas of continuous debris cover on Carbon and Emmons Glaciers; (c) slope angle computed from 3 m LiDAR-derived digital elevation model (DEM) of the debris-covered portion of Emmons Glacier; (d) slope angle for the gently-sloping portion of Carbon Glacier with continuous debris cover. [Colour figure can be viewed at wileyonlinelibrary.com]

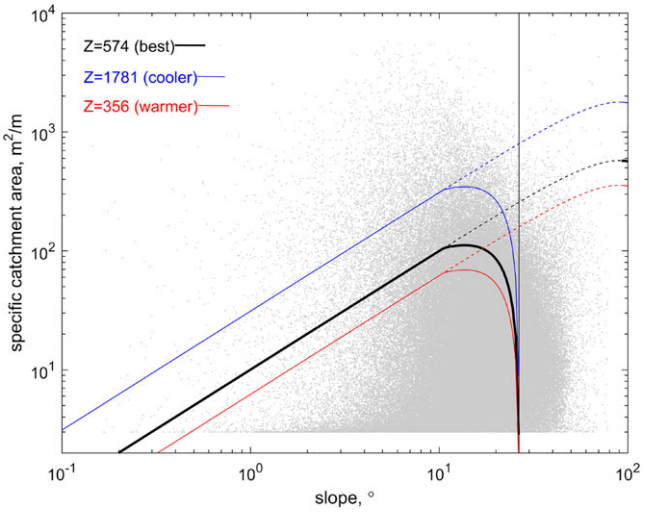


**Figure 5.** Plot of specific catchment area $a$ as a function of slope angle $\theta$ for the debris covered portion of Emmons Glacier's terminus (gray points). Superimposed are stability criteria 1 (vertical black line), 2 (dashed lines) and 3 (solid curves) for three different values of the parameter $Z$, where $Z = hK_s/\dot{m}$. Points falling above the criteria 2 and 3 curves or to the right of the line for criterion 1 are expected to be unstable for the supposed parameter values. Black lines correspond to best estimates for mean summer values at Emmons Glacier (see main text), while red corresponds to enhanced melt rates or reduced hydraulic transmissivity and blue lines correspond to reduced melt rates or increased transmissivity. [Colour figure can be viewed at wileyonlinelibrary.com]

loss or fluidization due to slope-normal seepage where $r_u = 1$. This mechanism depends on debris thickness (since $\dot{m}$ is a function of $h$) and hydraulic properties ($K_s$), both of which may vary substantially in space though without evident spatial patterns. The second mechanism arises from gravitational failure according to limit equilibrium in the presence of meltwater, which depends on several debris properties as well as slope and landscape position. The third mechanism is hydraulic erosion where the apparent depth of meltwater exceeds debris thickness, and this too depends on debris properties and landscape position.

From the mechanisms listed earlier, three distinct stability criteria are identified that can be evaluated from DEM data if debris properties are assumed to vary little in space:

1 simple limit equilibrium for an infinite slope with instability where $\tan\theta \geq \mu$;
2 hydraulic erosion from saturation-excess runoff where $d > h$, which can readily be estimated from the DEM data using Equation (9) with $a$ substituted for $s$;
3 gravitational slope failure of variably saturated debris according to Equation (11) with $F \leq 1$.

These criteria can be evaluated systematically across space and may thus be used to distinguish regions of greater risk for debris transport from slope and upslope-area rasters (e.g. Borga *et al.*, 1998). This is demonstrated here with reference to Emmons Glacier, but could readily be applied elsewhere provided enough observational constraints on debris thickness and texture.

To simplify the interpretation of these criteria, the parameter $Z$ (with dimensions [$L$]) is defined as:

$$Z = \frac{hK_s}{\dot{m}}, \tag{12}$$

or the ratio of debris transmissivity to meltwater supply rate (cf. Montgomery and Dietrich, 1994). Both criteria 2 and 3 can be stated as functions of $Z$ by substituting Equation (12) into Equations (9) and (11), respectively. The lines in Figure 5 identify hypothetical stability bounds (expressed as $a$ as a function of $\theta$) from all three criteria using reasonable – but spatially uniform – thickness and conductivity for supraglacial debris at Emmons Glacier. Figure 6 identifies areas of potential instability (criteria 1 and 3: pink and yellow) or erosion (criterion 2: blue) for the same set of conditions ($Z = 574$), amounting to a total of 10.5% of the debris-covered area for the illustrated case. Larger or smaller areas of the glacier would be susceptible to supraglacial debris transport under different values of $Z$, corresponding for example to warmer or cooler conditions, respectively.

The largest areas of expected gravitational instability indicated in Figure 6 are at known bare-ice exposures at a persistent ice-marginal cliff and a large meltwater-scoured gorge formed along the south margin of the glacier during a storm in 2006. Other areas with significant expected instability according to criteria 1 and 3 are along the face of the large medial moraine ridge near the glacier centerline, where debris is expected to move downslope to maintain debris mass balance as the moraine broadens with ablation (cf. Anderson, 2000). Areas of debris saturation (criterion 2 in blue) appear at the base of long slopes and in valleys between moraine ridges, consistent in general with observations of ponding, water-washed ice, and accumulation of water-sorted sediments in the field.

While the assumptions of uniform melt rate and debris properties implicit in defining the stability envelopes in Figure 5 and zones of debris transport in Figure 6 are clearly unrealistic, the analysis does appear to properly identify characteristic areas of instability and transport. Perhaps more importantly, these simplifications allow evaluation of the system's sensitivity to key parameters with large ranges of variability using the parameter $Z$.

## Discussion

Downwasting beneath debris requires both the gravitational settling of debris and the displacement and evacuation of generated meltwater. This leads to consideration of both the fluid pressure needed to convey the melted water away from the melting surface, and the downslope balance of meltwater on finite hillslopes. The result in Equation (3) suggests that substantial water pressures in excess of hydrostatic may be developed when ablation occurs at a rate $\dot{m}$ that approaches the debris hydraulic conductivity $K_s$. This effect may be negligible for $\dot{m}/K_s < 0.1$, but for higher values of this ratio, the effect may substantially reduce the stability of the debris.

The excess pressures derived from the simple ablation-settling model presented here are qualitatively similar to those resulting from the adaptation by Lawson (1982) and Paul and Eyles (1990) of the permafrost thaw-consolidation model. Suitability of the ablation-settling model relies on the assumption that a linear vertical pressure gradient is developed under the debris cover at it settles over ablating ice. Also implicitly assumed is that the surface slope is negligible so that seepage forces counteract gravity. Deviations from a linear gradient are likely where $K_s$ varies with depth in a debris layer, such as where fines have been preferentially translocated toward the debris–ice interface (e.g. Eyles, 1979). Additionally, evaporation or infiltration from the debris surface and development of unsaturated zones could all result in significant departures from the idealized pressure profiles assumed here. Simulating these departures, however, would require more

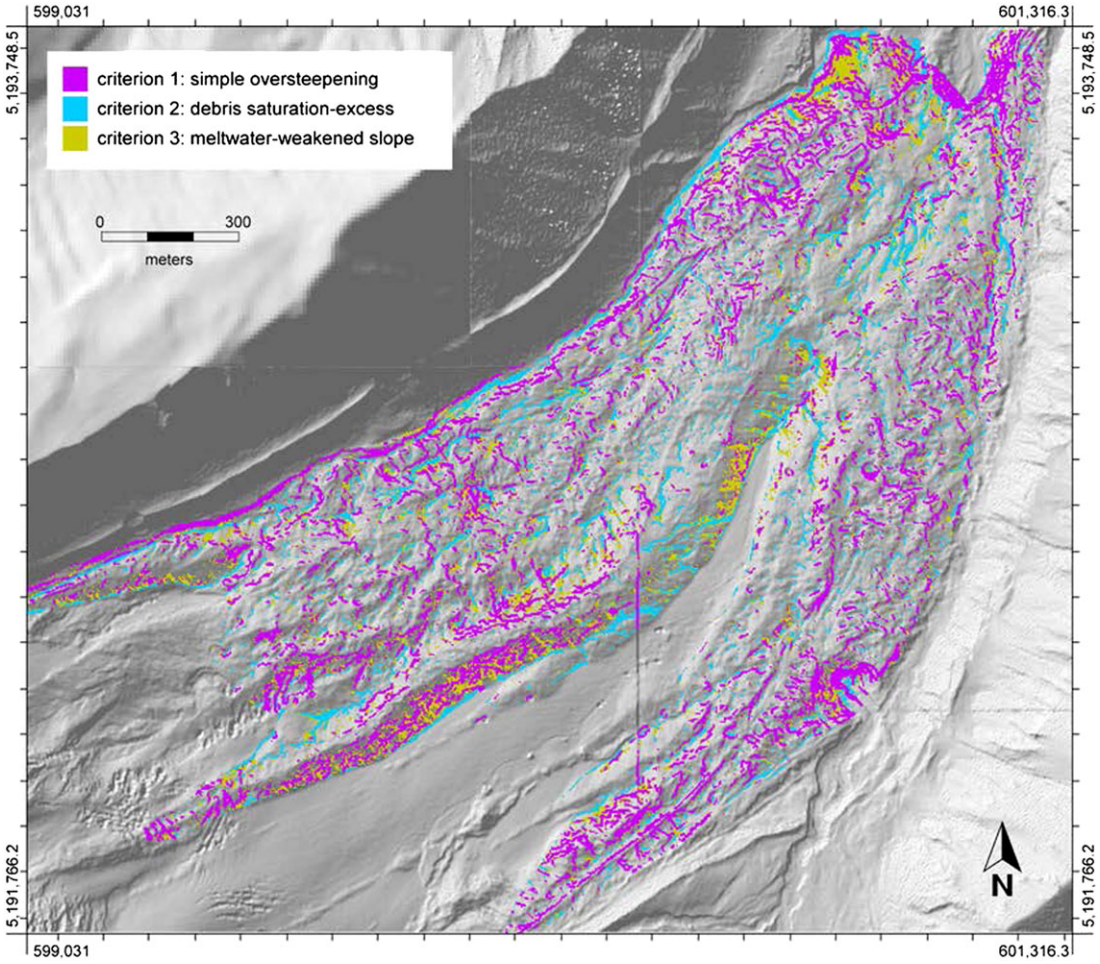


**Figure 6.** Map of the spatial distribution of areas meeting each of the criteria for instability under assumed parameter values ($Z = 574$; black curve in Figure 5). Criteria are (1) simple oversteepening; (2) saturation-excess; (3) meltwater-weakening, as discussed in the main text. [Colour figure can be viewed at wileyonlinelibrary.com]

sophisticated modeling that is beyond the scope of the present analysis.

Both $\dot{m}$and $K_s$ vary by orders of magnitude in debris-covered glacier settings. Long-term ablation rate depends in most cases on debris thickness, declining with increasing thickness as approximately $1/h$ (e.g. Reid and Brock, 2010). For example, field measurements during mid-summer 2013 and 2014 at Emmons Glacier (mean daily air temperature $T_s \sim 18°C$) suggested steady sub-debris melt rates on the order of 0.03 m/d for $h \sim 0.2$ m (Dits *et al.*, 2014). Measurements elsewhere indicate ablation rates ranging from negligible to more than 0.12 m/d under debris layers ranging from a few millimeters to more than 1 m (e.g. Nicholson and Benn, 2006). Debris hydraulic conductivity in glacial settings can range from $10^{-7}$ m/d (clay-rich till) to more than $10^{3}$ m/d (open-work gravel or cobbles) (Fetter, 1994). For silty sand with $K_s \sim 10^{-1}$ m/d, the ratio $\dot{m}/K_s \sim 1$ and instability by fluidization is likely even on gently-sloping surfaces, consistent with Lawson's observations at Matanuska Glacier (Lawson, 1979, 1982). For the sandy gravel that is observed over much of Emmons Glacier (which is inferred to have $K_s$ closer to $10^{2}$ m/d), $\dot{m}/K_s \sim 10^{-3}$ and fluidization is much more unlikely. Under these circumstances, excess pressure would be negligible; indeed the debris would have a tendency to be well-drained and water pressures within the debris would approach hydrostatic.

Textural differences may be important in both modern and ancient glacier settings, depending on debris sources and transport history. Where glaciers, for example in alpine settings, are fed coarse, weathering-resistant lithologies by rockfall, low values of the ratio $\dot{m}/K_s$ would promote rapid pore-water drainage and preclude the development of excess pore pressure or high water tables. In contrast, where glaciers acquire their supraglacial debris from inherently fine or extensively comminuted basal or aeolian sediments (e.g. some ancient ice sheet margins), $\dot{m}/K_s$ could be much higher and promote extensive instability and sediment fluidization in sufficiently warm climates.

The infinite slope analysis supports the expectation that slope angle is limited by the friction at the interface between the ice and overlying debris for well-drained debris. When the debris is fully saturated, the frictional resistance to slip may be reduced by more than half, making the maximum stable slope angle considerably smaller. For example, a saturated debris layer with moist bulk density $\rho_m = 2000$ kg/m$^3$ and hydrostatic pressure throughout produces $r_u = 0.5$. For these and related circumstances, the widely-applied infinite slope model with slope-parallel seepage is generally valid over a broad range of melt rates and hillslope settings (Equation (4)).

As the ratio $\dot{m}/K_s \sin\theta$ becomes larger, the debris may no longer be considered well-drained and pressures in excess of hydrostatic can arise at the base of the debris. The excess pressure determined by Equations (5) and (6) is that required to satisfy a steady-state two-dimensional water balance within a control volume. This pressure is sensitive in sloping terrain to the ratio $\dot{m}/K_s \sin\theta$ and is no longer negligible when this ratio exceeds $10^{-1}$. For a debris-covered glacier ablating at an average rate of 3 cm/d (0.03 m/d) during the summer melt season, this ratio takes a value of $10^{-1}$ for $K_s \sin\theta = 0.3$ m/d, which

for a 15° slope corresponds to $K_s \sim 1$ m/d, which is a reasonable value for clean sand. Coarser debris cover would permit sufficient pore pressure dissipation to limit excess pore pressures, but finer debris could become very unstable.

The dependence on $\dot{m}/K_s \sin\theta$ is clearly seen through the direct effect on ablation-settling, but it is important to note that $r_u$ is also influenced by slope angle and downslope position as it governs the steady value of $d$ at any point on a hillslope. The practical effect of the dependence of $\sin\theta$ is that instability can arise even in relatively conductive debris if the surface slope is insufficient to evacuate meltwater from the control volume as it is produced. Thus, slope angles in a particular debris type may be constrained on the high end by an effective slope angle threshold reduced by seepage and on the low end by inadequate meltwater drainage. However, the parameter space for which inadequate drainage causes gravitational instability at low slope angles is relatively small, as the pore space may tend to fill with water ($d = h$), resulting in ponding or overland runoff at smaller $a$.

The finite slope analysis provides an approximate means of identifying places on a supraglacial landscape where debris may become unstable. The stability fields illustrated in Figure 5 suggest that, for a given set of debris properties, there is a value of $a$ (or slope length $s$ for straight, planar slopes) above which the base of the slope becomes unstable. Shorter slopes, or those with smaller specific catchment areas, are conditionally stable unless impacted by additional forcing such as rainfall or snowmelt events. Longer slopes, however, should be unstable beginning a distance (or specific catchment area) $s$ ($a$) downslope.

Local destabilization of footslope debris may result in more widespread debris transport that extends upslope from the point at which $F = 1$. A relatively common occurrence in some debris-covered glacier settings is the progressive upslope migration of a 'failure front' as debris is removed by pore-water sapping. In this way, meeting the threshold value of $a$ that satisfies $F = 1$ may lead to more widespread destabilization upslope where the infinite slope idealization alone would predict $F > 1$.

If debris properties and melt rate on Emmons Glacier were uniformly equal to the values used to construct the black curve in Figure 5, the colored regions in Figure 6 would identify places on the glacier that should be subject to debris instability by one or more of the three stability criteria. Blue regions on the map represent places with fully-saturated debris and possible overland flow. Areas shaded yellow and pink would be susceptible to slip or debris-flow initiation. In all of the colored regions, instability would presumably move debris some distance downslope and leave behind bare ice. Although there are many ice cliffs and low-gradient outcrops of bare ice in wet swales on Emmons Glacier (as with most debris-covered glaciers), non-uniform distribution of debris thickness and permeability could account for departures from these predictions. For example, areas marked yellow or blue could remain stable and debris-covered if the debris there were coarser and/or thicker than the surroundings. Other deviations from the mapped zones of instability could reflect areas where the assumptions made here are violated, such as short slopes that exceed the threshold angle of criterion 1 without instability due to longitudinal buttressing from stable debris at the foot of the slope.

Because (all else being equal) $\dot{m}$ is inversely dependent upon $h$ in settings dominated by conductive heat transfer, $Z$ is particularly sensitive to changes in debris thickness. Increasing debris thickness by a factor of two affects melt rate, resulting in a four-fold increase in $Z$ and a corresponding four-fold increase in the slope length (or specific catchment area) that can remain stable. However, halving debris thickness results in a four-fold decrease in the stable slope length. Since many glaciers accumulate thicker debris blankets with transport downstream and/or elapsed ablation, this has implications for the broader scale spatial and temporal patterns of debris stability and transport across glaciers: where debris is on average thicker, $F$ will be greater for a given $a$ and $\theta$ and thus less likely to be destabilized. In contrast, where debris is thinner farther upglacier, $F$ will be smaller and debris instability more frequent and abundant. Stable debris will be limited to coarser materials on shorter or convex slopes that are insufficient to promote failure but sufficient to evacuate meltwater. The latter inference is consistent with the observation (e.g. Figures 4b and 5) that the most frequent and longest slopes on actively ablating debris-covered ice on Mount Rainier are around 10°–15°.

Some of the most rapid morphological changes in debris-covered glaciers occur on concave, convergent slopes such as those adjacent to supraglacial ponds or depressions (Pickard, 1983; Miles *et al.*, 2016; Watson *et al.*, 2016). On these slopes, meltwater flow through debris pore spaces converges and concentrates in a downslope direction. Because the slope angle decreases downslope meltwater accumulates to greater depth over shorter downslope distances than it would in straight or convex slopes. Other things being equal, debris would therefore be less stable on convergent and concave slopes than on convex or divergent slopes. In these concave, convergent slope settings, meltwater concentration may fully saturate debris at some distance downslope (indicated by the wetness index = 1), resulting either in ponding or supraglacial streamflow depending on whether a surface water outlet exists. Where a downslope surface-water outlet does exist, fluvial transport may play a significant role in debris transport given sufficient stream power. Destabilization of debris in such settings should promote lateral growth or migration of supraglacial channels and ponds, as well as accumulation of sediment in basins. The latter effect should promote establishment and growth of ice-walled lake deposits.

As indicated earlier, backwasting of debris-free ice cliffs is an important process in the ablation of debris-covered glaciers. Most actively-backwasting ice cliffs observed on Emmons Glacier in 2013–2014 are small (< 5 m in height) and of limited aerial extent. Elsewhere, debris-free ice cliffs are similarly of limited aerial extent (rarely exceeding a few percent of the area within largely debris-covered ice [Sakai *et al.*, 2002; Reid and Brock, 2014]) but can reach several tens of meters in height (Brun *et al.*, 2016; Watson *et al.*, 2017). Maintaining the dimensions of a retreating ice cliff requires that once debris is undercut by melting, it does not accumulate on the slope or form a wedge that protects the foot of the slope from further ablation. The model presented here provides some constraints on the dimensions and slope angles of backwasting cliffs that can remain unstable, depending on melt rates and debris hydraulic properties. For example, while it is certainly possible to undercut and mobilize coarse and highly permeable debris from atop an ice cliff, the coarse debris would likely stabilize and remain at the base of the ice cliff, insulating the cliff base and leading eventually to extinguishing of the ice cliff and cessation of backwasting. In finer debris with lower permeability, reduced water pressure dissipation and sustained instability at the footslope could allow evacuation of undercut debris from the base of a backwasting ice cliff, allowing sustained backwasting. This model prediction is consistent with observations in general, but could be easily tested in diverse settings.

There are several important limitations to the earlier mentioned analysis. The assumptions of spatially-uniform debris thickness, hydraulic conductivity, slope angle, and melt rate were made for analytical convenience, but could in principle be relaxed in a numerical scheme to allow for more realistic

system geometry and properties. Water inputs were assumed to be steady, and to be supplied strictly to the base of the debris by melting ice. Where debris thickness is small, sub-debris melt rates are not constant in time. As debris thickness grows, diurnal oscillations in meltwater production are dampened. Where melt-rate oscillations are substantial, the limit-equilibrium analysis above may be used with the peak melt rate to supply a conservative bound on debris stability. Alternatively, transient meltwater effects could be treated with a more rigorous, though complex, hillslope hydrology analysis. Similarly, transient effects on stability such as rainfall and snowmelt (inputs of water from above) and snow loading have been neglected. These effects could be explored more rigorously with suitable numerical methods, but their maximum possible impacts could be also assessed by choosing peak values (e.g. for elevated pore pressure resulting from rainfall infiltration).

The model presented here also addresses only the initiation of failure in supraglacial debris, and can provide no insight into the dynamics of downslope transport or deposition. The behavior of debris following mobilization should be governed by many of the same processes and variables that govern mass wasting in non-glacial settings (Iverson, 1997). The style of transport should depend on the interactions between debris and pore water, and between the mobilized mass and the ice substrate. The fate of mobilized debris should also depend in part on the topographic constraints of the evolving glacier surface (Denlinger and Iverson, 2001; Iverson and Denlinger, 2001). Debris deposition can be expected to occur where a change in slope, an increase in friction and/or decrease in fluid pressure can dissipate sufficient energy to arrest the moving debris mass (Iverson, 1997).

All of these mobilization and deposition processes and patterns result in local changes in the distribution of debris on the ice surface, which in turn affects the distribution of ablation. While the effects of non-uniform distribution of supraglacial debris on ablation are relatively well understood, there has been relatively little exploration of the longer-term feedback between relief production by differential melting and consequent debris mobilization. In general, we may expect that debris movement from the top to the base of a slope will enhance ablation rates at the top while subduing them at the base, leading to a reduction in slope angle or even a reversal of slope. The latter effect is essentially the key to topographic inversion – an essential process in landform genesis in glaciated landscapes influenced by high supraglacial debris loads (Clayton and Moran, 1974).

## Conclusions

Supraglacial debris has substantial impacts on the mass balance of glaciers as well as the sediments and landforms they leave behind. These impacts derive both from the differential ablation caused by non-uniform supraglacial debris distribution and from destabilization and transport of debris across a glacier surface. While the physics that govern differential ablation are relatively well-studied, the processes and variables that govern stability and transport of debris on a glacier surface have remained comparatively poorly known.

This paper identifies the key physical principles appropriate for assessing the gravitational stability of supraglacial debris on an actively-ablating glacier. Stability is assessed through a simplified limit-equilibrium analysis in the presence of steady-state seepage. A key consideration is the balance of meltwater within a supraglacial debris layer that is settling over ablating ice. Evacuation of meltwater from the ablating interface generates excess water pressures that become significant when the melt rate exceeds about 10% of the saturated hydraulic conductivity of the debris, causing reduced friction at the debris–ice interface. Where debris textures are fine and melt rates appreciable, debris–meltwater interaction can cause debris to be fully fluidized and unstable at any slope, or rigid but still unstable even on vanishingly-small slopes. Coarser or thicker debris should be less sensitive to meltwater interaction, remaining stable over a broader range of slope angles and configurations.

Meltwater accumulates with distance downslope as it moves by Darcian flow within a debris layer's pore space, reducing friction and supplying seepage forces. Using a simple model of downslope meltwater seepage, stability fields have been identified for different slope lengths and slope angles as a function of the ratio of melt rate to debris hydraulic conductivity ($\dot{m}/K_s$). The general relationships that follow from this model are consistent with observations on debris-covered glaciers, and make it possible to predict the location and extent of debris instability under different climate scenarios (e.g. increasing ablation rates). These relationships can also be leveraged to better understand how glacial sediments and landforms might differ between glaciers with diverse combinations of climate parameters and debris properties.

*Acknowledgements*—This project was supported in part by NSF-EAR-1225880. The author is grateful to Theresa Dits, Mariah Radue, Leah Nelson, Jayne Pasternak, and Justin Oelschlager for able field assistance at Emmons Glacier, to Andrew Fountain for logistical and moral support, and to Anders Schomacker and Ann Rowan for helpful reviews.

## References

Anderson L, Anderson R. 2016. Modeling debris-covered glaciers: response to steady debris deposition. *The Cryosphere* **10**: 1105–1124.

Anderson RS. 2000. A model of ablation-dominated medial moraines and the generation of debris-mantled glacier snouts. *Journal of Glaciology* **46**: 459–469. https://doi.org/10.3189/172756500781833025.

Barrette PD, Timco GW. 2008. Laboratory study on the sliding resistance of level ice and rubble on sand. *Cold Regions Science and Technology* **54**: 73–82. https://doi.org/10.1016/j.coldregions.2008.02.002.

Benn D, Evans D. 2010. *Glaciers and Glaciation*, second edn. Hodder Education: Abingdon.

Benn DI, Bolch T, Hands K, Gulley J, Luckman A, Nicholson LI, Quincey D, Thompson S, Toumi R, Wiseman S. 2012. Response of debris-covered glaciers in the Mount Everest region to recent warming, and implications for outburst flood hazards. *Earth-Science Reviews* **114**: 156–174. https://doi.org/10.1016/j.earscirev.2012.03.008.

Bennett GL, Evans DJA. 2012. Glacier retreat and landform production on an overdeepened glacier foreland: the debris-charged glacial landsystem at Kvíárjökull, Iceland. *Earth Surface Processes and Landforms* **37**: 1584–1602. https://doi.org/10.1002/esp.3259.

Bennett MR, Huddart D, Waller RI. 2000. Glaciofluvial crevasse and conduit fills as indicators of supraglacial dewatering during a surge, Skeidararjokull, Iceland. *Journal of Glaciology* **46**: 2–11.

Borga M, Dalla Fontana G, Da Ros D, Marchi L. 1998. Shallow landslide hazard assessment using a physically based model and digital elevation data. *Environmental Geology* **35**: 81–88.

Boulton GS. 1967. The development of a complex supraglacial morain at the margin of Sorbreen, Ny Friesland, Vestspitsbergen. *Journal Glaciology* **6**: 717–734.

Brun F, Buri P, Miles ES, Wagnon P, Steiner J, Berthier E, Ragaletti S, Kraaijenbrink P, Immerzeel WW, Pellicciotti F. 2016. Quantifying volume loss from ice cliffs on debris-covered glaciers using high-resolution terrestrial and aerial photogrammetry. *Journal of Glaciology* **62**: 684–695. https://doi.org/10.1017/jog.2016.54.

Casadei M, Dietrich WE, Miller NL. 2003. Testing a model for predicting the timing and location of shallow landslide initiation in soil-mantled landscapes. *Earth Surface Processes and Landforms* **28**: 925–950. https://doi.org/10.1002/esp.470.

Clayton L, Attig JW, Ham NR, Johnson MD, Jennings CE, Syverson KM. 2008. Ice-walled-lake plains: implications for the origin of hummocky glacial topography in middle North America. *Geomorphology* **97**: 237–248. https://doi.org/10.1016/j.geomorph.2007.02.045.

Clayton L, Moran SR. 1974. A glacial process-form model. In *Glacial Geomorphology*, Coates DR (ed). State University of New York: Binghamton, NY; 89–199.

Conway H, Rasmussen LA. 2000. Summer temperature profiles within supraglacial debris on Khumbu Glacier, Nepal. In *Debris-covered Glaciers*, Fountain AG, Nakawo M, Raymond CF (eds), IAHS Publication 264. IAHS Press: Wallingford; 89–97.

Denlinger RP, Iverson RM. 2001. Flow of variably fluidized granular masses across three-dimensional terrain: 2. Numerical predictions and experimental tests. *Journal of Geophysical Research: Solid Earth* **106**: 553–566. https://doi.org/10.1029/2000JB900330.

Dits T, Nelson L, Moore P. 2014. Small-scale Variations in Melt of the Debris-covered Emmons Glacier, Mount Rainier, USA. *Abstracts, AGU Fall Meeting: C31B–0296*.

Driscoll F. 1980. Wastage of the Klutlan ice-cored moraines, Yukon Territory, Canada. *Quaternary Research* **14**: 19–30.

Evans DJA. 2009. Controlled moraines: origins, characteristics and palaeoglaciological implications. *Quaternary Science Reviews* **28**: 183–208. https://doi.org/10.1016/j.quascirev.2008.10.024.

Evatt G, Abrahams I, Heil M, Mayer C, Kingslake J, Mitchell S, Fowler A, Clark C. 2015. Glacial melt under a porous debris layer. *Journal of Glaciology* **61**: 825–836.

Eyles N. 1979. Facies of supraglacial sedimentation on Icelandic and Alpine temperate glaciers. *Canadian Journal of Earth Sciences* **16**: 1341–1361.

Eyles N, Rogerson RJ. 1978. Sedimentology of medial moraines on Berendon Glacier, British Columbia, Canada: implications for debris transport in a glacierized basin. *Geological Society of America Bulletin* **89**: 1688–1693.

Fetter C. 1994. *Applied Hydrogeology*, third edn. Prentice-Hall: Upper Saddle River, NJ.

Gomez B, Small RJ. 1985. Medial moraines of the Haut Glacier d'Arolla, Valais, Switzerland: debris supply and implications for moraine formation. *Journal of Glaciology* **31**: 303–307.

Hambrey MJ. 1997. Genesis of "hummocky moraines" by thrusting in glacier ice: evidence from Svalbard and Britain. *Journal of the Geological Society* **154**: 623–632.

Hambrey MJ, Bennett MR, Dowdeswell J. 1999. Debris entrainment and transfer in polythermal valley glaciers. *Journal of Glaciology* **45**: 69–86.

Iverson RM. 1997. The physics of debris flows. *Reviews of Geophysics* **35**: 245–296.

Iverson RM, Denlinger RP. 2001. Flow of variably fluidized granular masses across three-dimensional terrain: 1. Coulomb mixture theory. *Journal of Geophysical Research: Solid Earth* **106**: 537–552. https://doi.org/10.1029/2000JB900329.

Johnson MD, Clayton L. 2005. Supraglacial landsystems in lowland terrain. In *Glacial Landsystems*, Evans DJA (ed). Arnold: London; 228–258.

Kirkbride MP, Deline P. 2013. The formation of supraglacial debris covers by primary dispersal from transverse englacial debris bands. *Earth Surface Processes and Landforms* **38**: 1779–1792. https://doi.org/10.1002/esp.3416.

Kjær KH, Krüger J. 2001. The final phase of dead-ice moraine development: processes and sediment architecture, Kötlujökull, Iceland. *Sedimentology* **48**: 935–952.

Korsgaard NJ, Schomacker A, Benediktsson ÍÖ, Larsen NK, Ingólfsson Ó, Kjær KH. 2015. Spatial distribution of erosion and deposition during a glacier surge: Brúarjökull, Iceland. *Geomorphology* **250**: 258–270. https://doi.org/10.1016/j.geomorph.2015.09.010.

Krüger J, Aber J. 1999. Formation of supraglacial sediment accumulations on Kötlujökull, Iceland. *Journal of Glaciology* **45**: 400–402.

Krüger J, Kjær K, Schomacker A. 2010. Dead-ice environments: a landsystems model for a debris-charged, stagnant lowland glacier margin, Kötlujökull. In *Developments in Quaternary Sciences*, Schomacker A, Krüger J, Kjær KH (eds). Elsevier: Amsterdam; 105–126.

Krüger J, Kjær KH. 2000. De-icing progression of ice-cored moraines in a humid, subpolar climate , Ko ¨ kull, Iceland. *Holocene* **6**: 737–747.

Lambe T, Whitman R. 1969. *Soil Mechanics*. John Wiley & Sons: New York.

Lawson DE. 1979. *Semdimentological Analysis of the Western Terminus Region of the Matanuska Glacier, Alaska (No. CRREL-79-9)*. Cold Regions Research and Engineering Lab: Hanover, NH.

Lawson DE. 1982. Mobilization, movement and deposition of active subaerial sediment flows, Matanuska Glacier, Alaska. *The Journal of Geology* **90**: 279–300.

Lindsay JB. 2016. Whitebox GAT: a case study in geomorphometric analysis. *Computers & Geosciences* **95**: 75–84. https://doi.org/10.1016/j.cageo.2016.07.003.

Lu N, Godt J. 2013. *Hillslope Hydrology and Stability*. Cambridge University Press: Cambridge.

McRoberts E, Morgenstern N. 1974a. Stability of slopes in frozen soil, Mackenzie Valley, NWT. *Canadian Geotechnical Journal* **11**: 554–573.

McRoberts E, Morgenstern N. 1974b. The stability of thawing slopes. *Canadian Geotechnical Journal* **11**: 447–469. https://doi.org/10.1139/t74-052.

Mihalcea C, Mayer C, Diolaiuti G, Agata CD, Smiraglia C, Lambrecht A, Vuillermoz E, Tartari G. 2008. Spatial distribution of debris thickness and melting from remote-sensing and meteorological data, at debris-covered Baltoro glacier, Karakoram, Pakistan. *Annals of Glaciology* **48**: 49–57.

Miles E, Pellicciotti F, Willis I, Steiner J. 2016. Refined energy-balance modelling of a supraglacial pond, Langtang Khola, Nepal. *Annals of Glaciology* **57**: 29–40.

Montgomery D, Dietrich W. 1994. A physically based model for the topographic control on shallow landsliding. *Water Resources Research* **30**: 1153–1171. https://doi.org/10.1029/93WR02979.

Moore PL, Iverson NR, Uno KT, Dettinger MP, Brugger KA, Jansson P. 2013. Entrainment and emplacement of englacial debris bands near the margin of Storglaciären, Sweden. *Boreas* **42**: 71–83. https://doi.org/10.1111/j.1502-3885.2012.00274.x.

Morgenstern NR, Nixon JF. 1971. One-dimensional consolidation of thawing soils. *Canadian Geotechnical Journal* **8**: 558–565. https://doi.org/10.1139/t71-057.

Muir Wood D. 2009. *Soil Mechanics: A One-dimensional Introduction*. Cambridge University Press: New York.

Nicholson L, Benn DI. 2006. Calculating ice melt beneath a debris layer using meteorological data. *Journal of Glaciology* **52**: 463–470. https://doi.org/10.3189/172756506781828584.

Nicholson L, Benn DI. 2013. Properties of natural supraglacial debris in relation to modelling sub-debris ice ablation. *Earth Surface Processes and Landforms* **38**: 490–501. https://doi.org/10.1002/esp.3299.

O'Loughlin EM. 1986. Prediction of surface saturation zones in natural catchments by topographic analysis. *Water Resources Research* **22**: 794–804. https://doi.org/10.1029/WR022i005p00794.

Østrem G. 1959. Ice melting under a thin layer of moraine, and the existence of ice cores in moraine ridges. *Geografiska Annaler* **41**: 228–230.

Paul MA, Eyles N. 1990. Constraints on the preservation of diamict facies (melt-out tills) at the margins of stagnant glaciers. *Quaternary Science Reviews* **9**: 51–69. https://doi.org/10.1016/0277-3791(90)90004-T.

Pickard J. 1983. Surface lowering of ice-cored moraine by wandering lakes. *Journal of Glaciology* **29**: 338–342.

Puget Sound LiDAR Consortium. 2009. LiDAR Remote Sensing Data Collection: Mount Rainier, WA. http://pugetsoundlidar.ess.washington.edu/lidardata/proj_reports/rainier_lidar_report.pdf [27 June 2017].

Reid TD, Brock BW. 2010. An energy-balance model for debris-covered glaciers including heat conduction through the debris layer. *Journal of Glaciology* **56**: 903–916. https://doi.org/10.3189/002214310794457218.

Reid TD, Brock BW. 2014. Assessing ice-cliff backwasting and its contribution to total ablation of debris-covered Miage glacier, Mont Blanc massif, Italy. *Journal of Glaciology* **60**: 3–13. https://doi.org/10.3189/2014JoG13J045.

Reznichenko N, Davies T, Shulmeister J, McSaveney M. 2010. Effects of debris on ice-surface melting rates: an experimental study. *Journal of Glaciology* **56**: 384–394. https://doi.org/10.3189/002214310792447725.

Reznichenko NV, Davies TRH, Alexander DJ. 2011. Effects of rock avalanches on glacier behaviour and moraine formation. *Geomorphology* **132**: 327–338. https://doi.org/10.1016/j.geomorph.2011.05.019.

Richardson SD, Reynolds JM. 2000. An overview of glacial hazards in the Himalayas. *Quaternary International* **65**: 31–47. https://doi.org/10.1016/S1040-6182(99)00035-X.

Rowan AV, Egholm DL, Quincey DJ, Glasser NF. 2015. Modelling the feedbacks between mass balance, ice flow and debris transport to predict the response to climate change of debris-covered glaciers in the Himalaya. *Earth and Planetary Science Letters* **430**: 427–438. https://doi.org/10.1016/j.epsl.2015.09.004.

Sakai A, Nakawo M, Fujita K. 2002. Distribution characteristics and energy balance of ice cliffs on debris-covered glaciers, Nepal Himalaya. *Arctic, Antarctic, and Alpine Research* **34**: 12. https://doi.org/10.2307/1552503.

Scherler D, Bookhagen B, Strecker MR. 2011. Spatially variable response of Himalayan glaciers to climate change affected by debris cover. *Nature Geoscience* **4**: 156–159. https://doi.org/10.1038/ngeo1068.

Schomacker A. 2008. What controls dead-ice melting under different climate conditions? A discussion. *Earth-Science Reviews* **90**: 103–113. https://doi.org/10.1016/j.earscirev.2008.08.003.

Schomacker A, Kjær K. 2007. Origin and de-icing of multiple generations of ice-cored moraines at Brúarjökull, Iceland. *Boreas* **36**: 411–425.

Schomacker A, Kjær KH. 2008. Quantification of dead-ice melting in ice-cored moraines at the high-arctic glacier Holmströmbreen, Svalbard. *Boreas* **37**: 211–225. https://doi.org/10.1111/j.1502-3885.2007.00014.x.

Selby M. 1993. *Hillslope Materials and Processes*. Oxford University Press: New York.

Sharp RP. 1949. Studies of superglacial debris on valley glaciers. *American Journal of Science* **247**: 289–315. https://doi.org/10.2475/ajs.247.5.289.

Shugar DH, Clague JJ. 2011. The sedimentology and geomorphology of rock avalanche deposits on glaciers. *Sedimentology* **58**: 1762–1783. https://doi.org/10.1111/j.1365-3091.2011.01238.x.

Shulmeister J, Davies TR, Evans DJA, Hyatt OM, Tovar DS. 2009. Catastrophic landslides, glacier behaviour and moraine formation – a view from an active plate margin. *Quaternary Science Reviews* **28**: 1085–1096. https://doi.org/10.1016/j.quascirev.2008.11.015.

Sisson T, Robinson J, Swinney D. 2011. Whole-edifice ice volume change AD 1970 to 2007/2008 at Mount Rainier, Washington, based on LiDAR surveying. *Geology* **39**: 639–642.

Spedding N. 2000. Hydrological controls on sediment transport pathways: implications for debris-covered glaciers. In *Debris-covered Glaciers*, Fountain AG, Nakawo M, Raymond CF (eds), IAHS Publication 264. IAHS Press: Wallingford; 133–142.

Takeuchi Y, Kayastha R, Nakawo M. 2000. Characteristics of ablation and heat balance in debris-free and debris-covered areas on Khumbu Glacier, Nepal Himalayas, in the pre-monsoon season. In *Debris-covered Glaciers*, Fountain AG, Nakawo M, Raymond CF (eds), IAHS Publication 264. IAHS Press: Wallingford; 53–61.

Talebi A, Troch PA, Uijlenhoet R. 2008. A steady-state analytical slope stability model for complex hillslopes. *Hydrological Processes* **22**: 546–553. https://doi.org/10.1002/hyp.6881.

Tarr R, Martin L. 1914. *Alaskan Glacier Studies of the National Geographic Society in the Yakutat Bay, Prince William Sound and Lower Copper River Regions*. National Geographic Society: Washington, DC.

Thompson S, Benn D, Dennis K, Luckman A. 2012. A rapidly growing moraine-dammed glacial lake on Ngozumpa Glacier, Nepal. *Geomorphology* **145–146**: 1–11.

Thompson S, Benn DI, Mertes J, Luckman A. 2016. Stagnation and mass loss on a Himalayan debris-covered glacier: processes, patterns and rates. *Journal of Glaciology* **62**: 467–485. https://doi.org/10.1017/jog.2016.37.

Vacco DA, Alley RB, Pollard D. 2010. Glacial advance and stagnation caused by rock avalanches. *Earth and Planetary Science Letters* **294**: 123–130. https://doi.org/10.1016/j.epsl.2010.03.019.

Watson C, Quincey D, Carrivick J, Smith M. 2016. The dynamics of supraglacial ponds in the Everest region, central Himalaya. *Global and Planetary Change* **142**: 14–27.

Watson C, Quincey D, Carrivick J, Smith M. 2017. Ice cliff dynamics in the Everest region of the central Himalaya. *Geomorphology* **278**: 238–251.

Watson R. 1980. Landform development on moraines of the Klutlan Glacier, Yukon Territory, Canada. *Quaternary Research* **14**: 50–59.

Westoby M, Dunning S, Hein A, Marrero S, Sugden DE. 2016. Interannual surface evolution of an Antarctic blue-ice moraine using multi-temporal DEMs. *Earth Surface Dynamics* **4**: 515–529.

Wright H. 1980. Surge moraines of the Klutlan Glacier, Yukon Territory, Canada: origin, wastage, vegetation succession, lake development, and application to the late-glacial of Minnesota. *Quaternary Research* **14**: 2–18.